Exploring Fluorescent Dyes at Biomimetic Interfaces with Second Harmonic Generation and Molecular Dynamics

Giuseppe Licari,[§] Lukasz Cwiklik,[†] Pavel Jungwirth,[‡] and Eric Vauthey[§]*

§ Department de physical chemistry, University of Geneva, 30 quai Ernest-Ansermet, CH-1211 Geneva 4, Switzerland.
† J. Heyrovsky Institute of Physical Chemistry, Czech Academy of Sciences, Prague
‡ Institute of Organic Chemistry and Biochemistry, Czech Academy of Sciences, Flemingovo nam. 2, 16610 Prague 6, Czech Republic

The adsorption of a DNA fluorescent probe belonging to the thiazole orange family at the dodecane/water and dodecane/phospholipid/water interfaces has been investigated using a combination of surface-second harmonic generation (SSHG) and all-atomistic molecular dynamics (MD) simulations. Both approaches point to a high affinity of the cationic dye for the dodecane/water interface with a Gibbs free energy of adsorption of the order of -45 kJ/mol. Similar affinity was observed with a monolayer of negatively charged DPPG lipids. On the other hand, no significant adsorption could be found with the zwitterionic DDPC lipids. This was rationalised in terms of Coulombic interactions between the monolayer surface and the cationic dye. The similar affinity for the interface with and without DDPG, despite the favourable Coulombic attraction in the latter case, could be explained after investigating the interfacial orientation of the dye. In the absence of monolayer, the dye adsorbs with its molecular plane almost flat at the interface, whereas in the presence of DPPG it has to intercalate into the monolayer and adopt a significantly different orientation to benefit from the electrostatic stabilisation.

Introduction

Liquid/water interfaces are ubiquitous in nature and are also playing key roles in many technological processes.[1-3] Because of the asymmetry of forces they experience, molecules in the interfacial region tend to adopt an orientation that is no longer isotropic contrary to those in the bulk phase. This confers to these interfaces properties that substantially depart from those of the two constituting bulk liquids.[4-11] As a consequence, chemical reactivity in such environment may substantially differ from that in solution phase.[12] This is exploited in the so-called 'on-water' organic synthesis, where reactions of hydrophobic reactants are strongly accelerated in the presence of water.[13-16] The latter effect is not only due to the specific properties of the interface itself but also to the anisotropic orientation of the adsorbed molecules, which can strongly facilitate intermolecular reactions with low steric factors. Similarly, the interfacial orientation of the adsorbates can enhance or prevent their aggregation relatively to bulk solutions.[17-20]

This orientation strongly depends on the structure of the adsorbate, on the presence of hydrophilic and lipophilic groups and on their location on the molecule. The presence and the nature of these groups also affect significantly the affinity of the molecule toward the interface. Adsorption of charged molecules at the interface can be influenced by the addition of salts into the aqueous phase.[21-24] For example, the concentration of the cationic dye malachite green at the alkane/water interface increases remarkably upon adding a salting-in anion such as thiocyanate.[24] This is due to the excess concentration of these anions at the interfacial region relatively to the bulk,[25-27] and thus to a Coulombic attraction of the oppositely charged dye. A similar effect was reported with the anionic surfactant sodium dodecyl sulphate (SDS) but only at concentrations lower than that required to form a monolayer.[28] Indeed, at higher SDS concentrations, this enhancement effect totally vanished and the population of absorbed dye was apparently similar to that without any surfactant. This was explained in terms of the competition for adsorption between the dye and SDS, that is strongly in favour of the latter given its strong amphiphilic nature. However, the effect of the presence of a surfactant monolayer at the interface on the adsorption of the dye was not further investigated. Such knowledge is particularly useful for our understanding of the interactions between the surface of membranes and molecules dissolved in the sub-phase.

We report here on our investigation on the adsorption properties of a dye in the presence of phospholipid monolayers at the dodecane/water interface. As phospholipids are the main

constituents of cell membranes, such dodecane/phospholipid/water combination can be considered as a simple but valuable model for investigating the interactions between the surface of biological membranes and water-soluble molecules. As a dye, we chose the cyanine dye **1** (**Chart 1**),[29] which belongs to the thiazole orange (TO) family of fluorescent DNA probes. This dye is also closely related to the yellow oxazole (YO) DNA-probe family,[30-31] several of which have recently been shown to have a high affinity toward the dodecane/water interface.[32-33] This affinity can be understood by considering that these DNA probes are soluble in water but have a high binding constant to DNA upon intercalation into the hydrophobic base-pair stack. The selected phospholipids are DPPC and DDPG (**Chart 1**), which have zwitterionic and anionic heads, respectively, whereas **1** bears a single positive charge. This allows the influence of Coulombic effects in the adsorption of the dye to be studied.

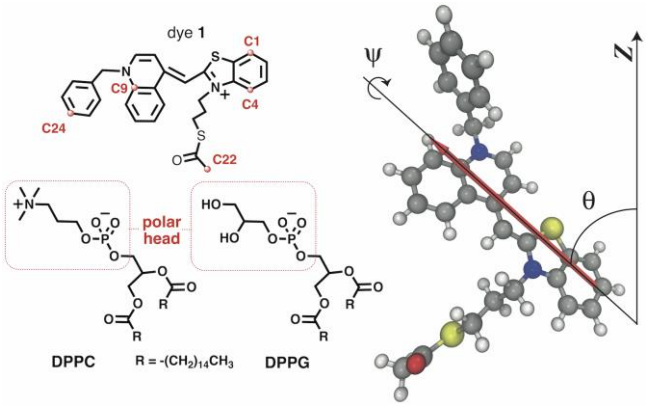

Chart 1: (Left) structure of dye **1** and of the DPPC and DPPG phospholipids. (Right) 3D representation of dye **1**, with the $S_1 \leftarrow S_0$ transition dipole moment (red arrow) and the Euler angles, θ and ψ (see text). The Z axis is normal to the interfacial plane.

For this investigation, we combined surface second harmonic generation (SSHG) and molecular dynamics (MD) simulations. SSHG is intrinsically surface selective, as the signal is directly proportional to the square modulus of the second-order susceptibility, $\chi^{(2)}$, which vanishes in centrosymmetric media, within the dipolar approximation.[34-35] Moreover, the SSHG signal is significantly resonantly enhanced when the probing wavelength coincides with one- or two-photon electronic transitions. This allows selective detection of adsorbates at low concentrations without interferences due to the non-resonant signal originating from the interface itself.[36] Furthermore, information on the orientation of the adsorbed molecules can be inferred from the analysis of polarisation-resolved SSHG measurements.[37-39] Previous SSHG studies of liquid-supported

surfactant monolayers have been mostly performed at air/liquid interfaces and were often directly probing the monolayer itself.[39-44] Similar direct probing of phospholipid monolayers at liquid interfaces was performed by vibrational sum-frequency generation (SFG).[11, 45-53] The study presented here differs substantially from these previous ones, because probing is done on the adsorbate, i.e. **1**, and not on the monolayer.

The absolute orientation of the dyes and the distribution of their orientation at the interface cannot be deduced from the SSHG data. This information was obtained here by performing atomistic MD simulations of **1** at the different interfaces. The aim of these simulations was also to rationalise the SSHG data and to obtain a microscopic picture of the interactions between the dye and these interfaces. Such a combination of SSHG spectroscopy and MD simulations is relatively well established.[54-59] However, to the best of our knowledge, it has never been applied to interfaces with phospholipid monolayers.

Methods

Samples

The dye **1**, 1-Benzyl-4-[(3-(3-acetylsulfanylpropyl)-2(3H)-benzothiazol-2-ylidene)methyl]quinolinium iodide, was obtained from T. Deligeorgiev (Faculty of Chemistry, University of Sofia) and used as received. Its synthesis has been described in detail in ref.[29]. The samples were freshly prepared from a 2 mM stock solution of dye in dimethyl sulfoxide (Acros Organics, spectroscopic grade). Dodecane (99+%) was purchased from Alfa Aesar. DPPC, 1,2-dipalmitoyl-*sn*-glycero-3-phosphocholine, and DPPG, 1,2-dipalmitoyl-*sn*-glycero-3-phospho-*rac*-(1-glycerol) sodium salt, were purchased from Sigma-Aldrich.

The SSHG samples for the dodecane/water interface experiments were prepared by (a) pouring 10 mL of an aqueous dye solution into a 4x4x4 cm^3 quartz cell and then (b) slowly adding 12 mL of dodecane. For the experiments with phospholipids, a specific amount of phospholipid was slowly deposited onto the lower aqueous phase with a syringe after step (a). The phospholipids were previously solubilized at 1 mM in a $CHCl_3$/methanol mixture (9/1 in volume). The area per lipid was estimated from the surface pressure-area isotherms provided in literature and recorded at air/buffer solution interfaces.[60] The pressure-area isotherms of phospholipids at air/water and oil/water interfaces were recently shown to be similar.[61] However, the area per lipid is only

approximate, because the total area of the sample in the quartz cell could not be determined precisely due to the meniscus.

For concentration-dependent SSHG measurements, the concentration was changed in situ by adding varying amounts of dye into the sample with a syringe and the final concentration was corrected for the dilution. The sample was stirred with a tiny magnetic stirrer for about 5 minutes after each dye addition. Since the number of adsorbed molecules is proportional to the amplitude of the second-harmonic field, the square root of the SSHG intensity was taken and the maximum of the resulting signal vs. concentration curve was normalized to 1, the maximum surface coverage. All experiments were performed at 294 ± 2 K.

Surface second harmonic generation

The SSHG setup has been described in detail previously.[20, 33] The probe pulses (~100 fs, ~0.7 μJ) centred at 1020 nm were generated by a collinear optical parametric amplifier (TOPAS-C, Light Conversion) pumped by the output of a Ti:Sapphire amplifier (Solstice, Spectra-Physics). This wavelength is close to the maximum of a SSHG band of **1**, which originates from a two-photon resonance with the $S_1 \leftarrow S_0$ transition.[32] The probe pulses were focused onto the sample by a 400 mm lens and hit the sample under total internal reflection condition with an angle of incidence of about 70°. The quadratic dependence of the signal was checked to ensure absence of higher-order processes (**Figure S11** in SI). No signal coming from the pure dodecane/water or dodecane/phospholipids/water interfaces could be detected in the absence of dye. The polarization of the probe beam was controlled with a half-wave plate, whereas the *p* (0°), *s* (90°) or *m* (45°) polarisation components of the second-harmonic signal were selected using a wire-grid polariser. Analysis of the polarization-resolved SSHG data was done as discussed previously,[33] and is described in detail in the SI.

Molecular dynamics simulations

Classical MD simulations were performed using the GROMACS 5.1.2 software.[62] The fully-atomistic AMBER99SB-ILDN force field (FF) was employed.[63-64] The standard TIP3P model was used for water,[65] whereas the phospholipids were described with the SLipids parameter set.[66-67] Initial GROMACS topology files for dodecane and **1** based on the AMBER force field were automatically generated by the Antechamber tool,[68] providing the Merz-Singh-Kollman

electrostatic potential[69] used for obtaining the partial charges in the restricted electrostatic potential approach (RESP).[70] The force field parameters of **1** were further refined using electronic structure calculations (see SI). For dodecane, Antechamber generated by default only two atom types, one for carbon and one for hydrogen. Since the default value of the Lennard-Jones potential depth ε was too large, dodecane was freezing at room temperature within 100 ns. Therefore, the dodecane atom types were changed to have the parameters ε and σ matching those from the work by Jämbeck and Lyubartsev,[67] where two different sets of carbon and hydrogen types were used for the CH_3 and CH_2 groups.

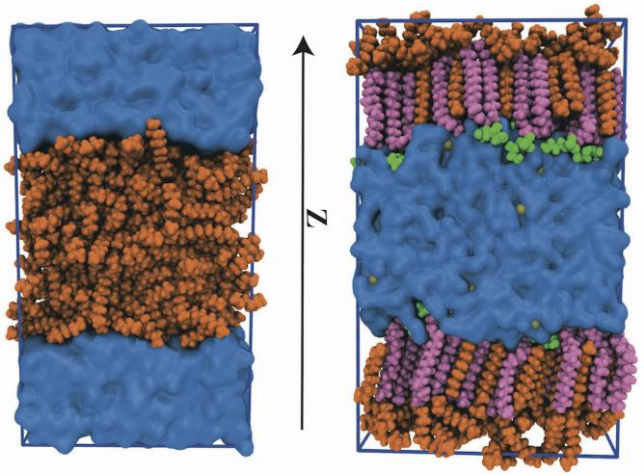

Figure 1. Examples of unit cells used for the MD simulations: dodecane/water (left) and dodecane/phospholipid/water (right). Each simulation box contains two distinct interfaces (blue: water; orange: dodecane; magenta: phospholipid tails; green: phospholipid heads; tan: partially visible ions).

A periodic rectangular box containing two distinct interfaces was used for the simulations (**Figure 1**). The exact number of molecules in each simulation is listed in **Table S2**. The isothermal-isobaric ensemble, NPT, was used for all production simulations involving the dodecane/water interface using the v-rescale thermostat at 295 K,[71] and the Parrinello-Rahman barostat with coupling constants of 0.5 ps and 3 ps respectively.[72] For interfaces with phospholipids, only the simulations at the maximum surface pressure were conducted in NPT. In the other cases, the simulations were performed at constant volume, NVT, to avoid departure from the prescribed area per lipid. Nevertheless, test simulations showed that the orientation of the dye was the same whether NPT or NVT conditions were adopted. To maintain analogous simulation conditions, the same settings for thermostat and barostat as for the dodecane/water interface were used in the phospholipid-

containing interface. The dodecane and water phases were separately coupled to the thermostat with the dyes, phospholipids, and ions in the water bath. For the interface simulations, a semi-isotropic pressure-coupling scheme was used. The coupled pressure in the Z direction (normal to the interfacial plane) was always 1 atm. The XY pressure for monolayer systems was also set to 1 atm., whereas for the dodecane/water interface, the XY pressure was set to a negative value between -40 and -85 atm in order to compensate for a large surface tension, which would cause explosion of the box in the Z direction. Empirical adjustment of this negative pressure was required, since increasing dye concentration at the interface decreased the surface tension. Non-bonded interactions were evaluated with a cut-off of 1.4 nm and long-range interactions were accounted for by the particle mesh Ewald method,[73] with 0.12 nm grid spacing and forth-order interpolation. Long-range dispersion correction for energy was also included. The LINCS algorithm[74] was used to constrain the bonds of all system components with the exception of water for which the SETTLE algorithm was applied.[75] The time step was set to 2 fs. Simulations were run for 200-600 ns and the first 100 ns were always considered as an equilibration period. The equilibration of the system was ensured by inspecting the total energy drift, the dye contacts with the interface and the density profiles at the two distinct interfaces of the box.

The Gibbs free energies of adsorption and of dimerization of **1** were deduced from one-dimensional potentials of mean force (PMF)[76] obtained using the umbrella sampling technique.[77-79] The reaction coordinate for the binding of the dye at the interface was the *Z*-axis of the simulation box. The reference species were the centre of mass (COM) of dodecane and DPPG, whose positions were already restrained with respect to the *Z*-axis since both dodecane and DPPG are not soluble in water. Each COM pull simulation was started after an equilibration MD, which terminated with the dye adsorbed at the interface. In the case of the dodecane/DPPG/water system, the area per DPPG was fixed to 70 $Å^2$ and **1** was found to intercalate into the DPPG monolayer, as discussed below.

In the case of the dimerization of **1**, a preliminary MD simulation was performed in pure water with two separate dye molecules. After a few ns, a stable dimer of **1** was formed and a suitable snapshot was selected as starting point for the pull simulation. Thus, one dye molecule was constrained to its position to serve as immobile reference, while the second dye molecule was pulled out from the dimer along the *Z* direction.

In all cases, the freely-moving dye was pulled for hundreds of ps using a spring constant of 1000 kJ mol^{-1} nm^{-2} and a pull rate of 0.01 nm ps^{-1}.[78] From the pull simulations, snapshots with COM separation of about 0.1 nm between the two species were extracted and used as starting point for the umbrella sampling. In each umbrella window, a MD simulation of 8 ns (for dodecane/DPPG/water) and 5 ns (for the other two systems) was performed and the bootstrapping procedure was repeated 200 times during the weighted histogram analysis method (WHAM) analysis. The PMF path was extracted from the probability distribution along the reaction coordinate obtained by umbrella sampling using WHAM.[80-81] The statistical error was estimated using the bootstrap method, also implemented in the GROMACS software. The error on the Gibbs free energies was retrieved from the errors at the maximum and minimum in the PMFs considering a confidence interval of two standard deviations.

Electronic structure calculations

Density Functional Theory (DFT) calculations were performed using Gaussian09 (rev. D)[82] to refine several parameters of the force field of **1** as described in detail in the SI. The optimized structure for the force field refinement was obtained at the B3LYP/6-311+G(d,p) level of theory,[83] using the implicit Polarized Continuum Model (PCM) representation for water.[84]

The vertical transition energies of **1** for the spectral simulations were calculated from time-dependent DFT (TD-DFT),[85-87] using either B3LYP or the long-range corrected CAM-B3LYP functional,[88] with the following functional parameters $\mu = 0.33$, $\alpha = 0.15$, and $\beta = 0.37$.[33]

Results and discussion

Affinity of the dye toward the interfaces

In previous studies,[32-33] the high interfacial affinity of YO DNA probes was mostly inferred from the high intensity of the SSHG signal as well as from various observations, such as the disruption of aggregates upon adsorption at the interface. Direct information is obtained here by measuring the adsorption isotherm of **1** at liquid/liquid interfaces by SSHG. Such measurements are usually performed at air/liquid interfaces.[55, 89-91], but the liquid/liquid interface is a better model of the membrane environment.

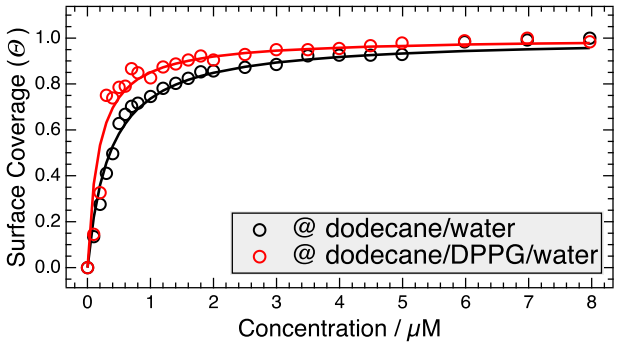

Figure 2. Adsorption isotherms of **1** at the dodecane/water and dodecane/DPPG/water interfaces measured by SSHG (66 Å^2/DPPG, 296 ± 0.5 K, *m* probe polarization, *s*-signal polarization component). The solid lines are the best fits of the Langmuir isotherm.

The strong adsorption of **1** at both dodecane/water and dodecane/DPPG/water interfaces is demonstrated by the adsorption isotherms depicted in **Figure 2**. In both cases, a significant SSHG signal could already be measured at ~0.1 μM bulk concentration of dye, a full dye coverage being achieved around 2 μM only. By contrast, the SSHG signal measured at the dodecane/DPPC/water interface at the same area/lipid (66 Å^2/DPPC) was too weak and unstable to construct an adsorption isotherm, pointing to a much lower affinity of **1** toward this interface.

The shape of the two isotherms suggests that the simple Langmuir model can be applied here.[89, 92] This model assumes that the interface is composed of identical and independent adsorption sites, which are all occupied at a surface coverage, Θ, of one. The adsorption isotherms in **Figure 2** can be safely used to determine the relative surface coverage because the orientation of the dye at both interfaces is independent of concentration as discussed below. This insures that the increase of the SSHG signal shown in **Figure 2** reflects the increasing surface coverage and does not originate from changes in the second-order response due to different dye orientations.[93] The free energies of adsorption at the interfaces without and with DPPG extracted from the isotherms amounts to -46.4 ± 0.3 kJ/mol and -48.2 ± 0.7 kJ/mol, respectively. This points to a large affinity of **1** towards both interfaces. Indeed, these values are substantially larger than that reported for the adsorption of indole at the air/DPPC/water interface (-34 kJ/mol),[42] or phenol and nitrophenol at the hexane/water interfaces (around -16 kJ/mol),[37] but are comparable to that measured with p-decylaniline at the air/water interface (-47 kJ/mol).[89] The affinity of **1** is not strongly affected by the presence of the DPPG monolayer at the interface and increases only very modestly relative to the bare dodecane/water interface. This small difference most probably results from counteracting

effects. In principle, Coulombic attraction of the cationic dye **1** toward the interface by the negatively charged heads of the DPPG monolayer should strongly favour adsorption.[21-24] However, access of **1** to the dodecane phase is largely prevented by the presence of the DPPG molecules. Moreover, the presence of the highly packed glycerol heads of DPPG may also introduce steric hindrance to the approach of **1** towards the phosphate group. The result of all these effects is a similar affinity of **1** for both dodecane/water and dodecane/DPPG/interfaces. By contrast, the presence of DPPC at the interface has a detrimental effect on the adsorption of **1**. Compared to DPPG, DPPC has a zwitterionic head with an ammonium end group that should lead to substantial Coulombic repulsion of the cationic dye from the interface. A qualitatively similar effect of the charge of the surfactant head on the SSHG signal from ionic dyes has recently been observed.[28]

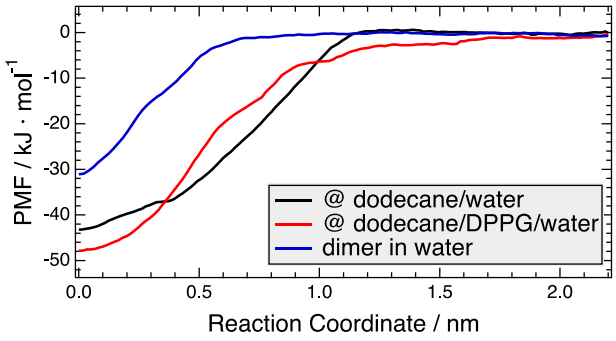

Figure 3. Potential of mean force (PMF) profiles for the adsorption of **1** at the dodecane/water and dodecane/DPPG/water interfaces (70 Å^2 /DPPG), and for the aggregation of **1** into a dimer in bulk water. For better visualization, the PMF curves were arbitrarily shifted along the reaction coordinate to match the PMF minima.

The free energy of adsorption of **1** at the dodecane/water and dodecane/DPPG/water interfaces obtained from the PMF profiles shown in **Figure 3** amounts to -43.8 ± 6.6 kJ/mol and -48.6 ± 4.4 kJ/mol, respectively. This excellent agreement between the SSHG results and the MD simulations supports the validity of both the model and the applied force field. The MD simulations also suggest that the interfacial affinity of **1** increases slightly in the presence of DPPG, although the free-energy difference is close to the statistical error.

Figure 3 also depicts the PMF profile for the formation of dimeric aggregates of **1** in water. The resulting free energy amounts to -31.1 ± 2.4 kJ/mol, a value close to those found experimentally for similar cyanine dyes.[94-96] Therefore, even though this large free energy of dimerization points

a strong propensity toward aggregation, this process is still energetically less favourable than adsorption at the interface. This preference for adsorption over aggregation does not preclude the formation of aggregates at sufficiently high concentration, as shown by the MD simulations discussed below and as found experimentally with the YO equivalent of dye **1**.

Besides the Gibbs free energies, the simulations also provide insight into the interactions between the dye and the interfaces. They clearly reveal that **1** either interacts with the polar phospholipid heads from the water phase, or intercalates into the phospholipid monolayer. This is illustrated in **Figure 4** where the density profiles of the individual constituents are shown for DPPG and DPPC monolayers with varying areas per phospholipid. Besides the normalised density of **1**, this figure also reports on the mass density of water, phospholipids and dodecane along the *Z*-axis of the unit cell. The *Z*=0 value coincides with the centre of the unit cell and only one half of the simulation box is shown for clarity. At high surface pressure, corresponding to a small area per lipid (47 $Å^2$), the dye cannot penetrate into the monolayer on the timescale of the simulations. In the case of DPPG, the dye experiences an electrostatic attraction towards the interface that favours a small accumulation at the interface relative to the bulk. It is worth noting that a fraction of dodecane molecules intercalates between the hydrophobic tails of the phospholipids and keep them in an ordered state. At lower surface pressure, i.e. at 60 $Å^2$/lipid, the dye starts to penetrate the DPPG monolayer but not the DPPC monolayer. The amount of dodecane intercalated between the phospholipid tails also increases. Finally, at the lowest surface pressure simulated, i.e. at 70 $Å^2$/lipid, the dye is fully located into the DPPG monolayer. However with DPPC, the dye remains almost entirely in the aqueous phase and exhibits a little excess concentration close to the water/DPPC interfacial region. The orientational analysis of these dyes close to the interface points to almost random orientation, in agreement with a weak SSHG signal (see Figure S9).

The effect of surface pressure on the adsorption of **1** has also been investigated by SSHG, upon varying the area/lipid from 66 to 47 $Å^2$. In the case of DPPG, an intense SSHG signal from **1** was measured within this whole range of area/lipid. By contrast with DPPC, a SSHG signal could only be detected at the largest area/lipid. However, as mentioned above, this signal was too weak and unstable for any reliable data to be recorded. Thus, both experiments and simulations give a very congruent picture of the adsorption of **1** with the DPPG but not the DPPC monolayer.

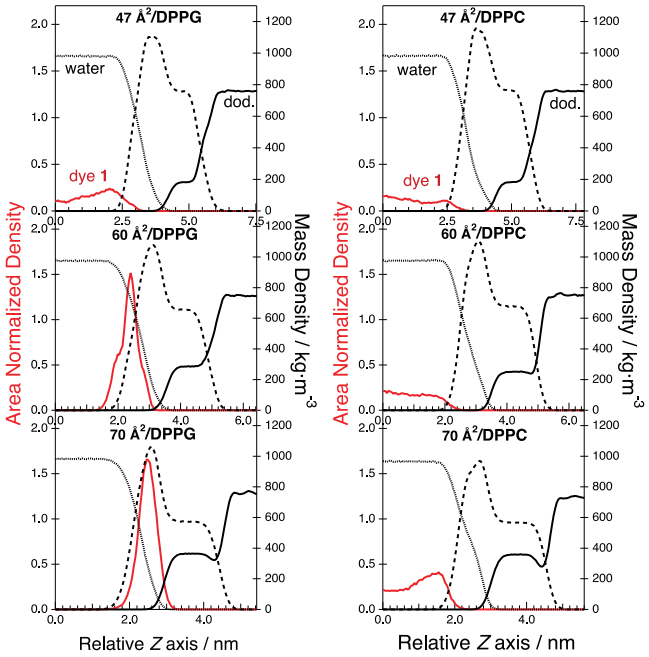

Figure 4. Density profiles obtained from simulations with a single molecule of dye **1** (red) at dodecane(solid)/phospholipid(dash)/water(dot) interfaces, using different areas/lipid. Left: DPPG; right: DPPC. Only one of the two interfaces of the box is shown for clarity.

Molecular orientation at the interfaces

Insight into the orientation of the adsorbed dye at the interfaces was obtained from polarisation-resolved SSHG measurements. In these experiments, different polarisation components of the SSHG signal, usually the *s* and *p* components, are recorded as a function of the polarisation of the probe field, γ. As discussed in detail in the SI and in ref. 35, 37-38, analysis of the resulting polarisation profiles allows the relative magnitude of the $\chi^{(2)}$ tensor elements to be determined. For liquid interfaces, only seven non-zero elements, three of which being independent, have to be considered: $c^{(2)}_{ZZZ}$, $c^{(2)}_{ZXX} = c^{(2)}_{ZYY}$, and $c^{(2)}_{XXZ} = c^{(2)}_{XZX} = c^{(2)}_{YZY} = c^{(2)}_{YYZ}$, where the subscripts are the Cartesian coordinates in the laboratory frame, with *X* and *Y* being in the interfacial plane, and *Y* and *Z* being in the incidence plane of the optical beam. Measurement of a third polarisation component, here 45°, gives access to the relative sign of these tensor elements.

The relative size and sign of these $\chi^{(2)}$ tensor elements depend on the hyperpolarisability tensor, β, of the species responsible for the SSHG signal (dye **1** in this case) and on its orientation:

$$\chi^{(2)} \propto N\langle\beta\rangle \qquad (1)$$

where N is the surface density, and the angle brackets indicate an average over the molecular orientations. Quantum-chemical calculations revealed that the hyperpolarisability tensor of a YO dye is dominated by a single element, β_{zzz}, where z is along the $S_1 \leftarrow S_0$ transition dipole moment, itself parallel to the main molecular axis.[33] We assume the same here for the structurally very similar dye **1**. In this case, the orientation parameter, D, can be calculated as:

$$D = \frac{\langle \cos^3 q \rangle}{\langle \cos q \rangle} = \frac{c^{(2)}_{ZZZ}}{c^{(2)}_{ZZZ} + 2\, c^{(2)}_{ZXX}} \qquad (2)$$

where θ is the tilt angle, i.e. the angle between the $S_1 \leftarrow S_0$ transition dipole moment of **1**, and the normal to the interface (axis Z, **Chart 1**). In the case of a very narrow distribution of orientations, for instance a Dirac δ distribution, D simplifies to $\cos^2\theta$ and the tilt angle can be readily obtained from the experiment. However, such situation where all the molecules adsorbed at the interface adopt an identical orientation is unlikely. Therefore a distribution has to be assumed in order to have a more realistic estimate of the mean tilt angle.

Because of the weakness of the SSHG signal with the DPPC monolayer, the polarisation-resolved measurements were carried out at the dodecane/water and dodecane/DPPG/water interfaces only. An area/DPPG of 66 Å^2 was used for all measurements. As showed by the pressure-area isotherm at air/buffer interface,[60] both liquid-expanded (LE) and liquid-condensed (LC) phases coexist in the monolayer at this area/lipid, corresponding to a surface pressure of ≈10 mN/m. Since a monolayer in a high compressed state is difficult to produce in our experiment, we chose to work in the LE/LC range.

An example of a polarization-resolved data is presented in **Figure 5**. The ensemble of data recorded at three output polarisations and six different dye concentrations (from 0.1 μM to 4 μM) is shown in **Figure S9**. It can immediately be seen that the polarization curves change markedly upon addition of DPPG, pointing to a different interfacial orientation of **1** in the presence of the lipid monolayer. The $\chi^{(2)}$ tensor elements extracted from these data were inserted into eq.(2) to calculate the D parameter at the different concentrations (**Table S5**). As shown in **Figure 6**, D, hence the interfacial orientation of the dye at both interfaces, remains constant within the whole concentration range.

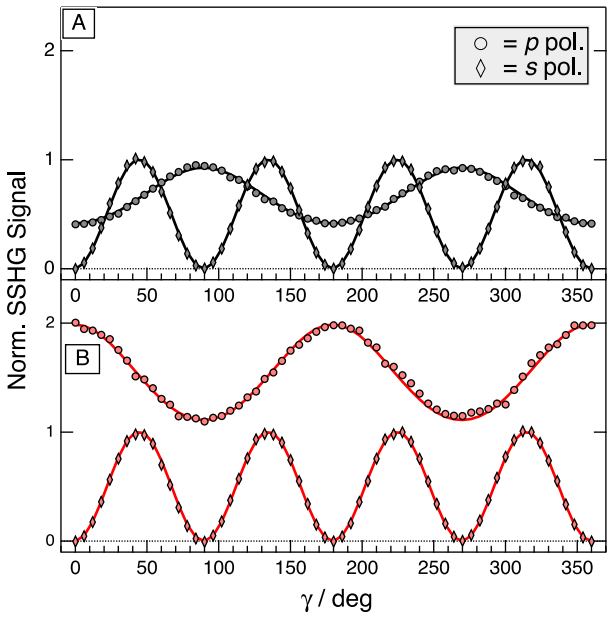

Figure 5. Polarization-resolved SSHG data recorded at two output polarizations with 2 μM of dye **1** at A) dodecane/water and B) dodecane/DPPG/water interfaces. The solid lines are the best-fit curves of eq.S5. Each set of data was normalized to the maximum of the *s* polarisation fit curve for better comparison.

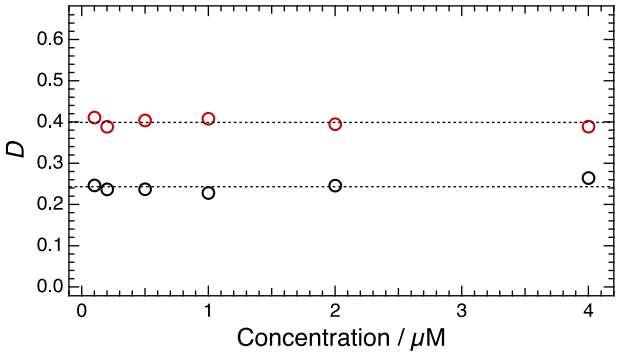

Figure 6. Orientation parameter *D* as a function of the bulk concentration of **1** for the dodecane/water (black) and dodecane/DPPG/water (red) interfaces. The horizontal lines pass through the average values.

The *D* parameter, averaged over the measurements at different concentrations, are listed in **Table 1**. Assuming a Dirac δ distribution of orientations, these values give tilt angles θ of approximately 60° and 50° for **1** at the dodecane/water and dodecane/DPPG/water, respectively (**Table 1**). The absolute direction of the dye at the interface, i.e. which of the two ends of the dye points away from the aqueous phase, cannot be inferred from the SSHG data, unless heterodyne detection is performed.[97-98] Therefore, the tilt angles could as well be equal to 120° and 130° without and with DPPG, respectively. The absolute orientation of **1** is difficult to predict on the basis of chemical

intuition, because **1** does not contain strongly hydrophilic or hydrophobic groups that could lead to a clear preferential orientation at the interface. The smaller tilt angle with DPPG indicates that the phospholipid monolayer induces a more perpendicular orientation of the dye long axis relative to the interface. However, a Dirac δ distribution is probably not realistic. Unfortunately, the distribution of dye orientations cannot be deduced from steady-state SSHG measurements.[56, 99] Therefore, we resorted to MD simulations to estimate the orientational distribution and the absolute orientation of the dye.

Table 1. Comparison of the experimental and simulated interfacial orientations of dye **1**.

	Dodecane/Water	**Dodecane/DPPG/Water**
experimental		
D [a]	0.243 ± 0.011	0.399 ± 0.009
$\theta(\delta)$ [b]	60.5° or 119.5° ± 0.7°	50.8° or 129.2° ± 0.5°
$\theta(\Delta\theta)$ [c]	74.2° or 105.8° ± 1.4°	54.5° or 125.5° ± 0.7°
simulated		
θ	88.7° ± 0.2°	110.6° ± 0.1°
$\Delta\theta$	38.0° ± 0.5°	27.3° ± 0.3°
ψ	87.6° ± 0.2°	75.7° ± 0.2°
$\Delta\psi$	48.4° ± 0.6°	40.7° ± 0.6°

a) D parameter averaged over concentration-dependent SSHG. b) Calculated assuming a Dirac δ distribution. c) Calculated assuming the simulated $\Delta\theta$ distribution.

We present first the MD results with **1** at the dodecane/water interface. These simulations were performed at different dye concentrations to mimic the SSHG experiments. For this, the number of dye molecules initially placed in the water phase was varied between 1 and 60. After equilibration, all dye molecules where adsorbed at one of the two interfaces of the simulation box. The surface concentration was then determined from the number of molecules adsorbed at each interface and varied from 0.025 to 0.57 dye/nm^2. As a comparison, the lowest surface concentration used for the SSHG experiments was estimated to be about 0.3 dye/nm^2 using the free energy of adsorption obtained experimentally. As the van der Waals area of the molecular plane of **1** is of the order of 1.4 nm^2 the surface concentration at full coverage should be lower than ~0.7 dye/nm^2.

Two Euler angles, namely the tilt angle θ and the rotation angle ψ (**Chart 1**) were extracted from the simulations. The rotation angle ψ is the angle between the Z laboratory axis and a vector located

in the molecular plane of **1** and perpendicular to its transition dipole moment. Therefore, ψ□ □° corresponds to the molecular plane being parallel to *Z*. The distributions of θ and ψ were analysed using a symmetric and a skewed Gaussian functions,[100] both functions giving similar results as discussed in the SI (**Figures S5** and **S6**). These two angles, as well as the full width at half maximum of their distribution, $\Delta\theta$ and $\Delta\psi$, are plotted as a function of surface concentration in **Figure 7**.

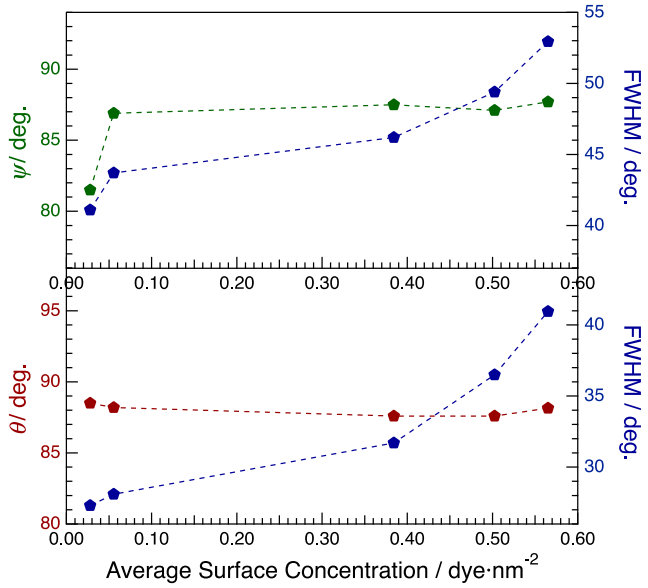

Figure 7. Orientation angles θ and ψ and corresponding distribution widths, $\Delta\theta$ and $\Delta\psi$, at the dodecane/water interface for different surface concentrations of **1** extracted from the MD simulations.

According to the simulations, the tilt angle θ angle is close to 90° and, since the $S_1 \leftarrow S_0$ transition dipole is essentially along the long molecular axis, **1** is lying almost flat at the interface (**Figure 8A**), with the benzothiazole end pointing on average slightly toward the aqueous phase. The tilt angle does not vary with concentration, in full agreement with the SSHG experiments. However, its distribution broadens from around 28° to 41° upon increasing the dye concentration. This result indicates that simulations using only one dye molecule could lead to inaccurate description of a real system. This broadening of the distribution is due to the increased interactions between nearby dye molecules and to the formation of transient aggregates that are in equilibrium with adsorbed monomers. These transient aggregates consist of H-type dimers with a parallel π-stacked conformation, with one constituent adsorbed at the interface as illustrated in

Figure 8B. A similar concentration dependence was obtained for the distribution of the rotational angle ψ, whose width increases by almost 15° along the concentration range. The main value of ψ stabilizes around 87° after a small initial rise from 82° upon going from one to two dye molecules. This implies that the molecular plane remains almost parallel to the interface at all concentrations.

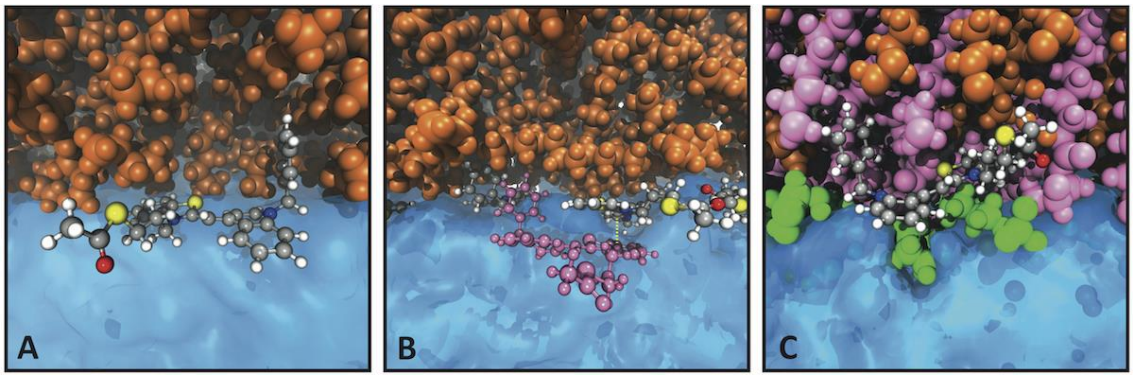

Figure 8. MD snapshots illustrating typical interfacial orientations of the dye: A) one and B) 40 dye molecules at the dodecane/water interface, and C) one dye molecule at the dodecane/DPPG/water interface (same colour code as in **Figure 1**). The B) snapshot shows an example of transient aggregation, with a pink-coloured dye molecule interacting through π-stacking with an adsorbed dye.

The increase of $\Delta\theta$ with concentration deduced from the MD simulations should lead to a ~15% increase of the *D* parameter.[35, 37-38] Such a change is close to the experimental limit of error on *D* and cannot be resolved here (**Figure 6**). However, an increase of *D* with increasing dye concentration was reported previously with YO derivatives.[33] There, the tilt angle was calculated from *D* assuming a Dirac δ distribution and was found to decrease with increasing concentration. However, the MD simulations performed here indicate that this increasing *D* could actually be due to an increase of $\Delta\theta$, and not to a variation of the average tilt angle.

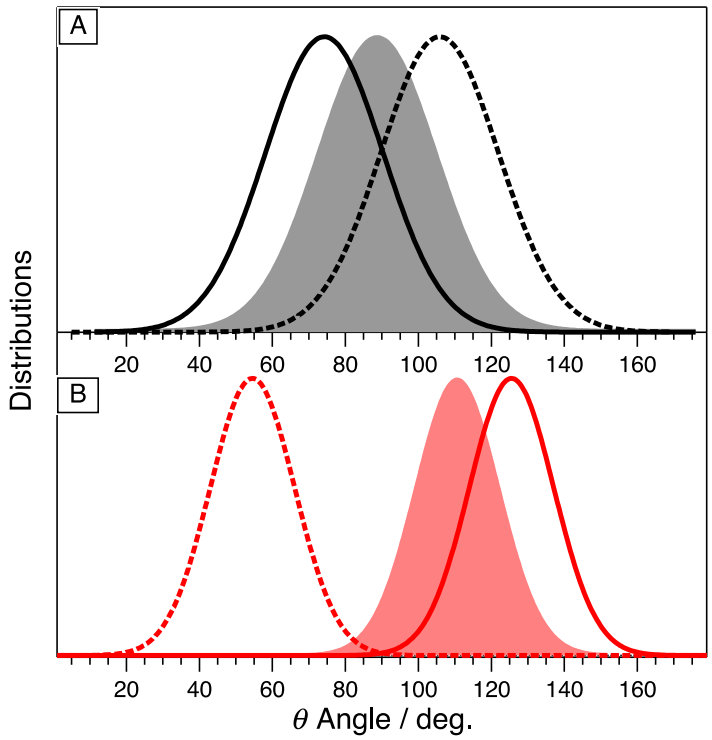

Figure 9. Comparison of the simulated (filled) and the two possible tilt angle distributions deduced from experiments (solid or dashed) of **1** at (A) dodecane/water and (B) dodecane/DPPG/water interfaces. The experimental distribution is assumed to be Gaussian with the same width as that obtained from the simulations.

To obtain better statistics, a MD simulation over 500 ns was performed with 40 dyes. The resulting θ and ψ values and the width of their distributions are listed in **Table 1**. These values are close to those extracted from the shorter simulations at similar surface concentration. The distribution of tilt angle obtained from this longer simulation was used to calculate the mean tilt angle from the experimentally measured *D* parameter. As shown in **Table 1**, the resulting angle amount to 74° vs. 60° as obtained assuming a Dirac δ distribution. This angle is also closer to that found by the MD simulations (**Figure 9**). However, given that the tilt angle obtained from the simulation is essentially distributed around 90 °, determination of the absolute orientation of **1** at the interface from *D* is not really possible. Therefore, a tilt angle distributed around 106° cannot be excluded. The discrepancy between the experimental and the MD values can be ascribed to imperfect parameterization of the dihedral angles of **1** (only three angles were refined) and/or of the force field of dodecane, both of which could lead to too flat an orientation of the dye. Nevertheless, the agreement is satisfactory and the MD model can now be used to rationalize the orientation of the

dye. The normalized densities along the *Z*-axis of dodecane, water, dye **1** and of two of its carbon atoms, C22 and C24 (see **Chart 1**), are reported in **Figure 10**. The density profile of the C22 atom, located at the end of the long side chain of **1**, is similar to that of the centre of mass of the whole dye. This indicates that the side chain does not penetrate into the dodecane, although it is predominantly hydrophobic. By contrast, the polarisation profile of C24 reveals that the benzyl is able to penetrate into the dodecane phase and is most probably responsible for the slight departure of the tilt angle from 90°. This effect is observed with both one and 40 dye molecules in the simulation box. However at high concentration, the density profiles associated with the dye exhibit a shoulder on the water side that is caused by the formation of transient aggregates.

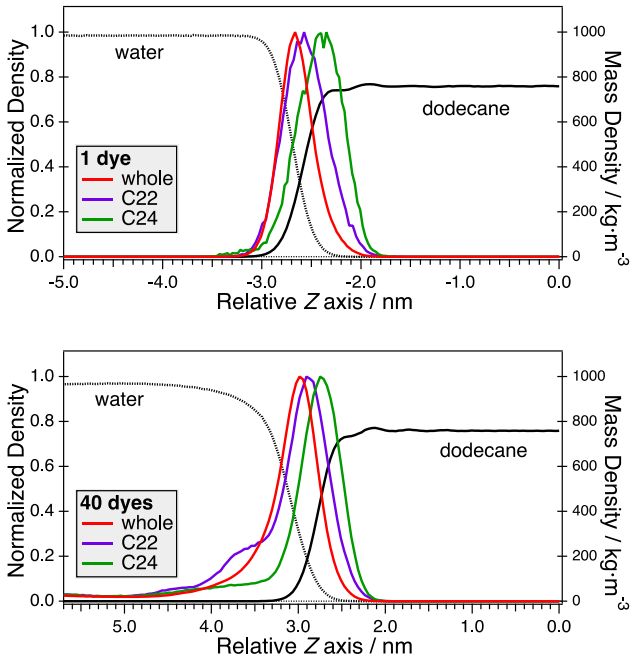

Figure 10. Density profiles of water and dodecane (right axis) and normalized density of **1** and of two of its atoms (left axis). The production MD goes from 100 to 200 ns. Only one interface of the box is shown for clarity.

Similar orientation analysis was carried out with the dodecane/DPPG/water interface but at only one dye concentration, because of the longer time required for the simulation. A 70 $Å^2$ area/DPPG, close to the experimental conditions, was used and the production simulation was extended to a total time of 600 ns. In this case again, the angle distributions could be well reproduced using Gaussian functions (**Figure S8**). **Table 1** reveals that the tilt angle of **1** in the presence of DPPG is almost 20° smaller than that predicted for the dodecane/water interface. A

very similar difference is observed for the θ values determined experimentally from *D*. Consequently, **1** orients more perpendicular to the interface in the presence of the DPPG monolayer (

Figure 8C). In this case however, the absolute orientation of the dye is unambiguous with the benzothiazole end clearly pointing away from the aqueous phase. The MD distribution of θ is showed in **Figure 9B** together with the experimental one derived from the average *D* parameter of 0.399 assuming a Gaussian distribution with a width of 27.3°.

The difference between the simulated and the experimental θ values is around 15° at both interfaces, suggesting a systematic error arising most probably from the parameterisation of the force field. Two other effects could be at the origin of this discrepancy in the case of the dodecane/DPPG/water interface: 1) the concentration of the K^+ counter-ions of DPPG close to the interface is unrealistically larger in the simulations, because of the very small volume of the aqueous phase in the box; 2) the estimation of the experimental surface pressure of the monolayer is only approximate. Since the dye intercalates into the monolayer, a small difference in the surface pressure could lead to a significant change in the orientation of the molecule.

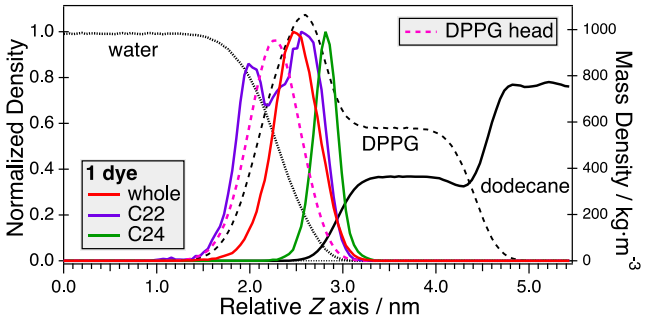

Figure 11. Density profiles of water, DPPG and dodecane (right axis) and normalized density of **1,** atoms C22, C24 and of the polar head of DPPG (left axis). The production MD goes from 100 to 300 ns. Only one interface of the box is shown for clarity.

The calculated normalized densities profiles of **1**, C22 and C24 at the dodecane/DPPG/water interface are depicted in **Figure 11**. The density profile of the polar head of DPPG is also reported for better visualisation of the position of the dye in the monolayer. It appears that **1** intercalates into the monolayer and localised just above the polar head of DPPG. This can be explained by the above-discussed Coulombic attraction of the cationic dye by the anionic polar head. In this case as well, the benzyl ring (C24) is pulled up towards the hydrophobic phase, consisting of the DPPG

tails and dodecane. Despite this, the chromophoric part of the dye is oriented with the benzothiazole toward the lipophilic phase, as shown in **Figure 8C**. The density profile of C22 exhibits two peaks, one at 1.3 Å from the average centre of mass of **1** similar to the dodecane/water interface, and a second at -4.8 Å, indicating that the thioester group can also extend towards the aqueous phase and orient perpendicular to molecular plane of **1**.

Therefore, both the SSHG measurements and the MD simulations point to substantial differences in the adsorption of **1** between the two interfaces, despite very similar affinities. The MD simulations confirm that the attractive Coulombic interaction exerted by the anionic head of DPPG is somehow compensated by the steric hindrance introduced by the lipids themselves. Therefore, the dye molecules have to intercalate into the monolayer to interact with the phosphate group of DPPG.

Conclusions

SSHG gives access to rich information on the adsorption of dyes at liquid interfaces and becomes particularly insightful when used in conjunction with MD simulations. This was shown here with the DNA probe **1**, belonging to the well-known thiazole orange (TO) family, at three different interfaces. SSHG allows direct and specific probing of the dye at the interface, whereas fully-atomistic MD simulations not only help rationalising the experimental results but provide a detailed molecular picture of the interface. Here two dodecane/phospholipid/water interfaces were used as a simple model of biological membranes, and more specifically of their surface, and were compared to the simple dodecane/water interface. Our results reveal the crucial role of the Coulombic interactions between the polar head of the lipids and the charged dye. The zwitterionic polar head of DPPC with the positive charge more exposed to the aqueous phase prevents adsorption of the cationic dye. The opposite effect is observed with the negatively charged DPPG, with a high affinity of the dye toward the interface, although not much larger that that for the interface without phospholipid. This modest increase of the interfacial affinity in the presence of DPPG, despite favourable Coulombic interactions, can be explained by fact that, in order to adsorb, the dye has to intercalate inside the monolayer, whereas it just adsorbs almost parallel to the dodecane/water interface. Consequently, the phospholipid monolayer introduces steric hindrance that counterbalances the Coulombic attraction.

Given the high interfacial affinity of this dye and its high binding constant to DNA, it will be particularly interesting to investigate the same systems with the presence of DNA in the aqueous phase. This could prove to be a peculiarly insightful approach toward a better understanding of membrane-DNA interactions, like for example in the case of membrane-associated DNA,[101-102] whose role is still not fully understood.

Acknowledgements

This work was supported by the Fonds National Suisse de la Recherche Scientifique through project No. 200020-165890 and the University of Geneva. G.L. wishes to thank Société Académique de Genève (Fond B. et E. Henneberg, n° 2016/27) for a travel grant to Prague in order to perform the Molecular Dynamics simulations. P.J. thanks the Czech Science Foundation for support via grant no. P208/12/G016.

1. Watarai, H.; Teramae, N.; Sawada, T., *Interfacial Nanochemistry*; Kluwer Academic: New York, 2005.
2. Ball, P., Water as an Active Constituent in Cell Biology. *Chem. Rev.* **2007**, *108*, 74-108.
3. Volkov, A. G. E., *Liquid Interfaces in Chemical, Biological, and Pharmaceutical Applications*; Marcel Dekker: New York, 2009.
4. Eisenthal, K. B., Liquid Interfaces. *Acc. Chem. Res.* **1993**, *26*, 636-43.
5. Wang, H.; Borguet, E.; Eisenthal, K. B., Polarity of Liquid Interfaces by Second Harmonic Generation Spectroscopy. *J. Phys. Chem. A* **1997**, *101*, 713-718.
6. Steel, W. H.; Walker, R. A., Measuring Dipolar Width across Liquid-Liquid Interfaces with 'Molecular Rulers'. *Nature* **2003**, *424*, 296-299.
7. Moore, F. G.; Richmond, G. L., Integration or Segregation: How Do Molecules Behave at Oil/Water Interfaces? *Acc. Chem. Res.* **2008**, *41*, 739-748.
8. Fita, P.; Punzi, A.; Vauthey, E., Local Viscosity of Binary Water+Glycerol Mixtures at Liquid/Liquid Interfaces Probed by Time-Resolved Surface Second Harmonic Generation. *J. Phys. Chem. C* **2009**, *113*, 20705-20712.
9. Fita, P.; Fedoseeva, M.; Vauthey, E., Hydrogen-Bond-Assisted Excited-State Deactivation at Liquid/Water Interfaces. *Langmuir* **2011**, *27*, 4645-4652.
10. Richert, S.; Fedoseeva, M.; Vauthey, E., Ultrafast Photoinduced Dynamics at Air/Liquid and Liquid/Liquid Interfaces. *J. Phys. Chem. Lett.* **2012**, *3*, 1635-1642.
11. Kundu, A.; Yamaguchi, S.; Tahara, T., Evaluation of Ph at Charged Lipid/Water Interfaces by Heterodyne-Detected Electronic Sum Frequency Generation. *J. Phys. Chem. Lett.* **2014**, *5*, 762-766.
12. Piradashvili, K.; Alexandrino, E. M.; Wurm, F. R.; Landfester, K., Reactions and Polymerizations at the Liquid–Liquid Interface. *Chem. Rev.* **2016**, *116*, 2141-2169.
13. Breslow, R., Hydrophobic Effects on Simple Organic Reactions in Water. *Acc. Chem. Res.* **1991**, *24*, 159-164.

14. Gajewski, J. J., The Claisen Rearrangement. Response to Solvents and Substituents: The Case for Both Hydrophobic and Hydrogen Bond Acceleration in Water and for a Variable Transition State. *Acc. Chem. Res.* **1997**, *30*, 219-225.
15. Narayan, S.; Muldoon, J.; Finn, M. G.; Fokin, V. V.; Kolb, H. C.; Sharpless, K. B., "On Water": Unique Reactivity of Organic Compounds in Aqueous Suspension. *Angew. Chem., Int. Ed.* **200**5, *44*, 3275-3279.
16. Shapiro, N.; Vigalok, A., Highly Efficient Organic Reactions "on Water", "in Water", and Both. *Angew. Chem., Int. Ed.* **2008**, *47*, 2849-2852.
17. Fujiwara, K.; Wada, S.; Monjushiro, H.; Watarai, H., Ion-Association Aggregation of an Anionic Porphyrin at the Liquid/Liquid Interface Studied by Second Harmonic Generation Spectroscopy. *Langmuir* **2006**, *22*, 2482-2486.
18. Yao, H.; Ikeda, H.; Kitamura, N., Surface Induced J Aggregation of Pseudoisocyanine Dye at a Glass/Solution Interface Studied by Total-Internal-Reflection Fluorescence Spectroscopy. *J. Phys. Chem. B* **1998**, *102*, 7691.
19. Sen, S.; Yamaguchi, S.; Tahara, T., Different Molecules Experience Different Polarities at the Air/Water Interface. *Angew. Chem. Int. Ed.* **2009**, *48*, 6439-6442.
20. Fedoseeva, M.; Letrun, R.; Vauthey, E., Excited-State Dynamics of Rhodamine 6g in Aqueous Solution and at the Dodecane/Water Interface. *J. Phys. Chem. B* **2014**, *118*, 5184-5193.
21. Steinhurst, D. A.; Baronavski, A. P.; Owrutsky, J. C., Transient Second Harmonic Generation from Oxazine Dyes at the Air/Water Interface. *J. Phys. Chem. B* **2002**, *106*, 3160-3165.
22. Beildeck, C. L.; Liu, M. J.; Brindza, M. R.; Walker, R. A., Solvation of P-Nitrophenol at a Water/Alkane Interface: The Role of Ionic Strength and Salt Identity. *J. Phys. Chem. B* **2005**, *109*, 14604-14610.
23. Punzi, A.; Martin-Gassin, G.; Grilj, J.; Vauthey, E., Effect of Salt on the Excited-State Dynamics of Malachite Green in Bulk Aqueous Solutions and at Air/Water Interfaces: A Femtosecond Transient Absorption and Surface Second Harmonic Generation Study. *J. Phys. Chem. C* **2009**, *113*, 11822-11829.
24. Fedoseeva, M.; Fita, P.; Punzi, A.; Vauthey, E., Salt Effect on the Formation of Dye Aggregates at Liquid/Liquid Interfaces Studied by Time-Resolved Surface Second Harmonic Generation. *J. Phys. Chem. C* **2010**, *114*, 13774-13781.
25. Jungwirth, P.; Tobias, D. J., Specific Ion Effects at the Air/Water Interface. *Chem. Rev.* **2006**, *106*, 1259-1281.
26. Pegram, L. M.; Record Jr, M. T., Quantifying Accumulation or Exclusion of H+, Ho-, and Hofmeister Salt Ions near Interfaces. *Chem. Phys. Lett.* **2008**, *467*, 1-8.
27. Zhang, Y.; Cremer, P. S., Chemistry of Hofmeister Anions and Osmolytes. *Annu. Rev. Phys. Chem.* **2011**, *61*, 63-83.
28. Fedoseeva, M.; Fita, P.; Vauthey, E., Excited-State Dynamics of Charged Dyes at Alkane/Water Interfaces in the Presence of Salts and Ionic Surfactants. *Langmuir* **2013**, *29*, 14865-14872.
29. Deligeorgiev, T.; Gadjev, N.; Vasilev, A.; Drexhage, K.-H.; Yarmoluk, S. M., Synthesis of Novel Monomeric and Homodimeric Cyanine Dyes with Thioacetyl Substituents for Nucleic Acid Detection. *Dyes Pigm.* **2006**, *70*, 185-191.
30. Glazer, A. N.; Rye, H. S., Stable Dye-DNA Intercalation Complexes as Reagents for High Sensitivity Fluorescencec Detection. *Nature* **1992**, *359*, 859-861.
31. Fürstenberg, A.; Deligeorgiev, T. G.; Gadjev, N. I.; Vasilev, A. A.; Vauthey, E., Structure-Fluorescence Contrast Relationship in Cyanine DNA Intercalators: Toward Rational Dye Design? . *Chem. Eur. J.* **2007**, *13*, 8600-8609.

32. Licari, G.; Vauthey, E., Ultrafast Excited-State Dynamics at Interfaces: Fluorescent DNA Probes at the Dodecane/Water Interface. *Proc. SPIE, Physical Chemistry of Interfaces and Nanomaterials XIV* **2015**, *9549*, 95490M.
33. Licari, G.; Brevet, P.-F.; Vauthey, E., Fluorescent DNA Probes at Liquid/Liquid Interfaces Studied by Surface Second Harmonic Generation. *Phys. Chem. Chem. Phys.* **2016**, *18*, 2981-2992.
34. Eisenthal, K. B., Liquid Interfaces Probed by Second-Harmonic and Sum-Frequency Spectroscopy. *Chem. Rev.* **1996**, *96*, 1343-1360.
35. Brevet, P.-F., *Surface Second Harmonic Generation*; Presses polytechniques et universitaires romandes: Lausanne, 1997.
36. Fedoseeva, M.; Richert, S.; Vauthey, E., Excited-State Dynamics of Organic Dyes at Liquid-Liquid Interfaces. *Langmuir* **2012**, *28*, 11291-11301.
37. Tamburello-Luca, A. A.; Hébert, P.; Brevet, P. F.; Girault, H. H., Resonant-Surface Second-Harmonic Generation Studies of Phenol Derivatives at Air/Water and Hexane/Water Interfaces. *J. Chem. Soc., Faraday Trans.* **1996**, *92*, 3079-3085.
38. Simpson, G. J.; Westerbuhr, S. G.; Rowlen, K. L., Molecular Orientation and Angular Distribution Probed by Angle-Resolved Absorbance and Second Harmonic Generation. *Anal. Chem.* **2000**, *72*, 887-898.
39. Martin-Gassin, G.; Benichou, E.; Bachelier, G.; Russier-Antoine, I.; Jonin, C.; Brevet, P. F., Compression Induced Chirality in Dense Molecular Films at the Air/Water Interface Probed by Second Harmonic Generation. *J. Phys. Chem. C* **2008**, *112*, 12958-12965.
40. Kotaro, K.; Hideo, T.; Atsuo, F., Symmetry and Second-Order Susceptibility of Hemicyanine Monolayer Studied by Surface Second-Harmonic Generation. *Jpn. J. Appl. Phys.* **1991**, *30*, 1050.
41. Teerenstra, M. N.; Hagting, J. G.; Schouten, A. J.; Nolte, R. J. M.; Kauranen, M.; Verbiest, T.; Persoons, A., Second-Harmonic Generation from Floating Monolayers and Langmuir−Blodgett Multilayers of Poly(Isocyanide)S. *Macromol.* **1996**, *29*, 4876-4879.
42. Mitchell, S. A., Indole Adsorption to a Lipid Monolayer Studied by Optical Second Harmonic Generation. *J. Phys. Chem. B* **2009**, *113*, 10693-707.
43. Matsuoka, Y.; Taguchi, D.; Manaka, T.; Iwamoto, M., Visualizing Polarization Structure of Lipid Langmuir Monolayer by Surface Second-Harmonic Generation Technique. *Thin Solid Films* **2014**, *554*, 8-12.
44. Lv, K.; Lin, L.; Wang, X.; Zhang, L.; Guo, Y.; Lu, Z.; Liu, M., Significant Chiral Signal Amplification of Langmuir Monolayers Probed by Second Harmonic Generation. *J. Phys. Chem. Lett.* **2015**, *6*, 1719-23.
45. Bonn, M.; Roke, S.; Berg, O.; Juurlink; Stamouli, A.; Müller, M., A Molecular View of Cholesterol-Induced Condensation in a Lipid Monolayer. *J. Phys. Chem. B* **2004**, *108*, 19083-19085.
46. Liu, J.; Conboy, J. C., Asymmetric Distribution of Lipids in a Phase Segregated Phospholipid Bilayer Observed by Sum-Frequency Vibrational Spectroscopy. *J. Phys. Chem. C* **2007**, *111*, 8988-8999.
47. Ohe, C.; Goto, Y.; Noi, M.; Arai, M.; Kamijo, H.; Itoh, K., Sum Frequency Generation Spectroscopic Studies on Phase Transitions of Phospholipid Monolayers Containing Poly(Ethylene Oxide) Lipids at the Air-Water Interface. *J. Phys. Chem. B* **2007**, *111*, 1693-1700.
48. Lis, D.; Guthmuller, J.; Champagne, B.; Humbert, C.; Busson, B.; Peremans, A.; Cecchet, F., Vibrational Sum-Frequency Generation Activity of a 2,4-Dinitrophenyl Phospholipid Hybrid Bilayer: Retrieving Orientational Parameters from a Dft Analysis of Experimental Data. *ChemPhysChem* **2013**, *14*, 1227-1236.

49. Johnson, C. M.; Baldelli, S., Vibrational Sum Frequency Spectroscopy Studies of the Influence of Solutes and Phospholipids at Vapor/Water Interfaces Relevant to Biological and Environmental Systems. *Chem. Rev.* **2014**, *114*, 8416-8446.
50. Li, B.; Lu, X.; Han, X.; Wu, F.-G.; Myers, J. N.; Chen, Z., Interfacial Fresnel Coefficients and Molecular Structures of Model Cell Membranes: From a Lipid Monolayer to a Lipid Bilayer. *J. Phys. Chem. C* **2014**, *118*, 28631-28639.
51. Wei, F.; Xiong, W.; Li, W.; Lu, W.; Allen, H. C.; Zheng, W., Assembly and Relaxation Behaviours of Phosphatidylethanolamine Monolayers Investigated by Polarization and Frequency Resolved Sfg-Vs. *Phys. Chem. Chem. Phys.* **2015**, *17*, 25114-22.
52. Feng, R.-J.; Li, X.; Zhang, Z.; Lu, Z.; Guo, Y., Spectral Assignment and Orientational Analysis in a Vibrational Sum Frequency Generation Study of Dppc Monolayers at the Air/Water Interface. *J. Chem. Phys.* **2016**, *145*, 244707/1-244707/11.
53. Takeshita, N.; Okuno, M.; Ishibashi, T.-a., Molecular Conformation of Dppc Phospholipid Langmuir and Langmuir-Blodgett Monolayers Studied by Heterodyne-Detected Vibrational Sum Frequency Generation Spectroscopy. *Phys. Chem. Chem. Phys.* **2017**, Ahead of Print.
54. Petersen, P. B.; Saykally, R. J.; Mucha, M.; Jungwirth, P., Enhanced Concentration of Polarizable Anions at the Liquid Water Surface: Shg Spectroscopy and Md Simulations of Sodium Thiocyanate. *J. Phys. Chem. B* **2005**, *109*, 10915-21.
55. Miller, A. E.; Petersen, P. B.; Hollars, C. W.; Saykally, R. J.; Heyda, J.; Jungwirth, P., Behavior of Beta-Amyloid 1-16 at the Air-Water Interface at Varying Ph by Nonlinear Spectroscopy and Molecular Dynamics Simulations. *J. Phys. Chem. A* **2011**, *115*, 5873-80.
56. Kundu, A.; Watanabe, H.; Yamaguchi, S.; Tahara, T., Agreement between Experimentally and Theoretically Estimated Orientational Distributions of Solutes at the Air/Water Interface. *J. Phys. Chem. C* **2013**, *117*, 8887-8891.
57. Richert, S.; Mosquera Vazquez, S.; Grzybowski, M.; Gryko, D. T.; Kyrychenko, A.; Vauthey, E., Excited-State Dynamics of an Environment-Sensitive Push–Pull Diketopyrrolopyrrole: Major Differences between the Bulk Solution Phase and the Dodecane/Water Interface. *J. Phys. Chem. B* **2014**, *118*, 9952-9963.
58. Loison, C.; Nasir, M. N.; Benichou, E.; Besson, F.; Brevet, P. F., Multi-Scale Modeling of Mycosubtilin Lipopeptides at the Air/Water Interface: Structure and Optical Second Harmonic Generation. *Phys. Chem. Chem. Phys.* **2014**, *16*, 2136-48.
59. Svechkarev, D.; Kolodezny, D.; Mosquera-Vazquez, S.; Vauthey, E., Complementary Surface Second Harmonic Generation and Molecular Dynamics Investigation of the Orientation of Organic Dyes at a Liquid/Liquid Interface. *Langmuir* **2014**, *30*, 13869−13876.
60. Travkova, O. G.; Brezesinski, G., Adsorption of the Antimicrobial Peptide Arenicin and Its Linear Derivative to Model Membranes--a Maximum Insertion Pressure Study. *Chem. Phys. Lipids* **2013**, *167-168*, 43-50.
61. Saint Martin, E.; Konovalov, O.; Daillant, J., Studies of Phospholipid Monolayer at Liquid/Liquid Interface in Presence of an Antimicrobial Peptide. *Thin Solid Films* **2007**, *515*, 5687-5690.
62. Abraham, M. J.; Murtola, T.; Schulz, R.; Páll, S.; Smith, J. C.; Hess, B.; Lindahl, E., Gromacs: High Performance Molecular Simulations through Multi-Level Parallelism from Laptops to Supercomputers. *SoftwareX* **2015**, *1-2*, 19-25.
63. Lindorff-Larsen, K.; Piana, S.; Palmo, K.; Maragakis, P.; Klepeis, J. L.; Dror, R. O.; Shaw, D. E., Improved Side-Chain Torsion Potentials for the Amber Ff99sb Protein Force Field. *Proteins* **2010**, *78*, 1950-8.

64. Hornak, V.; Abel, R.; Okur, A.; Strockbine, B.; Roitberg, A.; Simmerling, C., Comparison of Multiple Amber Force Fields and Development of Improved Protein Backbone Parameters. *Proteins* **2006**, *65*, 712-25.
65. Jorgensen, W. L.; Chandrasekhar, J.; Madura, J. D.; Impey, R. W.; Klein, M. L., Comparison of Simple Potential Functions for Simulating Liquid Water. *J. Chem. Phys.* **1983**, *79*, 926-935.
66. Jambeck, J. P.; Lyubartsev, A. P., An Extension and Further Validation of an All-Atomistic Force Field for Biological Membranes. *J. Chem. Theory Comput.* **2012**, *8*, 2938-48.
67. Jambeck, J. P.; Lyubartsev, A. P., Derivation and Systematic Validation of a Refined All-Atom Force Field for Phosphatidylcholine Lipids. *J. Phys. Chem. B* **2012**, *116*, 3164-79.
68. Wang, J.; Wang, W.; Kollman, P. A.; Case, D. A., Automatic Atom Type and Bond Type Perception in Molecular Mechanical Calculations. *J. Mol. Graph. Model.* **2006**, *25*, 247-60.
69. Singh, U. C.; Kollman, P. A., An Approach to Computing Electrostatic Charges for Molecules. *J. Comput. Chem.* **1984**, *5*, 129-145.
70. Bayly, C. I.; Cieplak, P.; Cornell, W. D.; Kollman, P. A., A Well-Behaved Electrostatic Potential Based Method Using Charge Restraints for Deriving Atomic Charges: The Resp Model. *J. Phys. Chem.* **1993**, *97*, 10269-10280.
71. Bussi, G.; Zykova-Timan, T.; Parrinello, M., Isothermal-Isobaric Molecular Dynamics Using Stochastic Velocity Rescaling. *J. Chem. Phys.* **2009**, *130*, 074101.
72. Parrinello, M.; Rahman, A., Polymorphic Transitions in Single-Crystals - a New Molecular-Dynamics Method. *J. Appl. Phys.* **1981**, *52*, 7182-7190.
73. Darden, T.; York, D.; Pedersen, L., Particle Mesh Ewald: An N X Log(N) Method for Ewald Sums in Large Systems. *J. Chem. Phys.* **1993**, *98*, 10089-10092.
74. Hess, B.; Bekker, H.; Berendsen, H. J. C.; Fraaije, J. G. E. M., Lincs: A Linear Constraint Solver for Molecular Simulations. *J. Comput. Chem.* **1997**, *18*, 1463-1472.
75. Miyamoto, S.; Kollman, P. A., Settle: An Analytical Version of the Shake and Rattle Algorithm for Rigid Water Models. *J. Comput. Chem.* **1992**, *13*, 952-962.
76. Roux, B., The Calculation of the Potential of Mean Force Using Computer Simulations. *Comput. Phys. Commun.* **1995**, *91*, 275-282.
77. Torrie, G. M.; Valleau, J. P., Nonphysical Sampling Distributions in Monte Carlo Free-Energy Estimation: Umbrella Sampling. *J. Comput. Phys.* **1977**, *23*, 187-199.
78. Lemkul, J. A.; Bevan, D. R., Assessing the Stability of Alzheimer's Amyloid Protofibrils Using Molecular Dynamics. *J. Phys. Chem. B* **2010**, *114*, 1652-60.
79. Hub, J. S.; Winkler, F. K.; Merrick, M.; de Groot, B. L., Potentials of Mean Force and Permeabilities for Carbon Dioxide, Ammonia, and Water Flux across a Rhesus Protein Channel and Lipid Membranes. *J. Am. Chem. Soc.* **2010**, *132*, 13251-63.
80. Hub, J. S.; de Groot, B. L.; van der Spoel, D., G_Wham—a Free Weighted Histogram Analysis Implementation Including Robust Error and Autocorrelation Estimates. *J. Chem. Theory Comput.* **2010**, *6*, 3713-3720.
81. Kumar, S.; Rosenberg, J. M.; Bouzida, D.; Swendsen, R. H.; Kollman, P. A., The Weighted Histogram Analysis Method for Free-Energy Calculations on Biomolecules. I. The Method. *J. Comput. Chem.* **1992**, *13*, 1011-1021.
82. Frisch, M. J., et al. *Gaussian 09 (Rev. D)*, Gaussian, Inc.: Wallingford, CT, USA, **2009**.
83. Lee, C.; Yang, W.; Parr, R. G., Development of the Colle-Salvetti Correlation-Energy Formula into a Functional of the Electron Density. *Phys. Rev. B* **1988**, *37*, 785-789.

84. Marenich, A. V.; Cramer, C. J.; Truhlar, D. G., Universal Solvation Model Based on Solute Electron Density and on a Continuum Model of the Solvent Defined by the Bulk Dielectric Constant and Atomic Surface Tensions. *J. Phys. Chem. B* **2009**, *113*, 6378-6396.
85. Bauernschmitt, R.; Ahlrichs, R., Treatment of Electronic Excitations within the Adiabatic Approximation of Time Dependent Density Functional Theory. *Chem. Phys. Lett.* **1996**, *256*, 454-464.
86. Stratmann, R. E.; Scuseria, G. E.; Frisch, M. J., An Efficient Implementation of Time-Dependent Density-Functional Theory for the Calculation of Excitation Energies of Large Molecules. *J. Chem. Phys.* **1998**, *109*, 8218-8224.
87. Scalmani, G.; Frisch, M. J.; Mennucci, B.; Tomasi, J.; Cammi, R.; Barone, V., Geometries and Properties of Excited States in the Gas Phase and in Solution: Theory and Application of a Time-Dependent Density Functional Theory Polarizable Continuum Model. *J. Chem. Phys.* **2006**, *124*, 94107.
88. Yanai, T.; Tew, D. P.; Handy, N. C., A New Hybrid Exchange-Correlation Functional Using the Coulomb-Attenuating Method (Cam-B3lyp). *Chem. Phys. Lett.* **2004**, *393*, 51-57.
89. Castro, A.; Bhattacharyya, K.; Eisenthal, K. B., Energetics of Adsorption of Neutral and Charged Molecules at the Air/Water Interface by Second Harmonic Generation: Hydrophobic and Solvation Effects. *J. Chem. Phys.* **1991**, *95*, 1310-1315.
90. Song, J.; Kim, M. W., Second Harmonic Generation Study of Malachite Green Adsorption at the Interface between Air and an Electrolyte Solution: Observing the Effect of Excess Electrical Charge Density at the Interface. *J. Phys. Chem. B* **2010**, *114*, 3236-3241.
91. Subir, M.; Eltouny, N.; Ariya, P. A., A Surface Second Harmonic Generation Investigation of Volatile Organic Compound Adsorption on a Liquid Mercury Surface. *RSC Adv.* **2015**, *5*, 23464-23470.
92. Limousin, G.; Gaudet, J. P.; Charlet, L.; Szenknect, S.; Barthès, V.; Krimissa, M., Sorption Isotherms: A Review on Physical Bases, Modeling and Measurement. *Appl. Geochem.* **2007**, *22*, 249-275.
93. Higgins, D. A.; Byerly, S. K.; Abrams, M. B.; Corn, R. M., Second Harmonic Generation Studies of Methylene Blue Orientation at Silica Surfaces. *J. Phys. Chem.* **1991**, *95*, 6984-6990.
94. Neumann, B.; Pollmann, P., Investigation of Two Cyanine Dyes at Normal and High Pressure by Uv/Vis Spectroscopy. *Phys. Chem. Chem. Phys.* **2000**, *2*, 4784-4792.
95. Chibisov, A. K., Photonics of Dimers of Cyanine Dyes. *High Energy Chem.* **2007**, *41*, 200-209.
96. Ahmadi, S.; Deligeorgiev, T. G.; Vasilev, A.; Kubista, M., The Dimerization Study of Some Cationic Monomethine Cyanine Dyes by Chemometrics Method. *Russ. J. Phys. Chem. A* **2012**, *86*, 1974-1981.
97. Yamaguchi, S.; Tahara, T., Heterodyne-Detected Electronic Sum Frequency Generation: "Up" Versus "Down" Alignment of Interfacial Molecules. *J. Chem. Phys.* **2008**, *129*, 101102.
98. Nihonyanagi, S.; Mondal, J. A.; Yamaguchi, S.; Tahara, T., Structure and Dynamics of Interfacial Water Studied by Heterodyne-Detected Vibrational Sum-Frequency Generation. *Annu. Rev. Phys. Chem.* **2014**, *64*, 579-603.
99. Rao, Y.; Hong, S.-Y.; Turro, N. J.; Eisenthal, K. B., Molecular Orientational Distribution at Interfaces Using Second Harmonic Generation. *J. Phys. Chem. C* **2011**, *115*, 11678-11683.
100. Rusch, P. F.; Lelieur, J. P., Analytical Moments of Skewed Gaussian Distribution Functions. *Anal. Chem.* **1973**, *45*, 1541-1543.
101. Lerner, R. A.; Meinke, W.; Goldstein, D. A., Membrane-Associated DNA in the Cytoplasm of Diploid Human Lymphocytes. *Proc Natl Acad Sci U S A* **1971**, *68*, 1212-6.

102. Cheng, J.; Torkamani, A.; Peng, Y.; Jones, T. M.; Lerner, R. A., Plasma Membrane Associated Transcription of Cytoplasmic DNA. *Proc Natl Acad Sci U S A* **2012**, *109*, 10827-31.